Two-dimensional transition metal phosphides as cathode additive in robust lithium-sulfur batteries

Jie Zhang,[†] *Dawei Yang,*[*,†] *Canhuang Li,*[Δ] *Qianhong Gong,*[†] *Wei Bi,*[†] *Xuejiao Zheng,*[&] *Jordi Arbiol,*[‡,⊥] *Shengjun Li,*[†] *Andreu Cabot*[*,⊥,Δ]

[†] Henan Key Laboratory of Quantum Materials and Quantum Energy, School of Quantum Information Future Technology, Henan University, Kaifeng, 475004, China.

[Δ] Catalonia Institute for Energy Research – IREC, Sant Adrià de Besòs, Barcelona, 08930, Spain.

[&] Nanjing Hydraulic Research Institute, Nanjing 210029, China

[‡] Catalan Institute of Nanoscience and Nanotechnology (ICN2), CSIC and BIST Campus UAB, Bellaterra, 08193 Barcelona, Spain.

[⊥] ICREA, Pg. Lluís Companys 23, 08010, Barcelona, Spain.

Email: dwyang@henu.edu.cn

Email: acabot@irec.cat

Abstract

The development of advanced cathode materials able to promote the sluggish redox kinetics of polysulfides is crucial to bringing lithium-sulfur batteries to the market. Herein, two electrode materials: namely Zr_2PS_2 and Zr_2PTe_2, are identified through screening several hundred thousand compositions in the Inorganic Crystal Structure Database. First-principles calculations are performed on these two materials. These structures are similar to that of the classical MXenes. Concurrently, calculations show

Zr_2PS_2 and Zr_2PTe_2 possess high electrical conductivity, promoted Li ion diffusion, and excellent electrocatalytic activity for the Li-S reaction and particularly for the Li_2S decomposition. Besides the mechanisms behind the excellent predicted performance of Zr_2PS_2 and Zr_2PTe_2 are elucidated through electron localization function, charge density difference, and localized orbital locator. This work not only identifies two candidate sulfur cathode additives but may also serve as a reference for the identification of additional electrode materials in new generations of batteries, particularly in sulfur cathodes.

Keywords: Lithium-sulfur batteries, cathode materials, phosphides, screening, designing

Materials databases such as the Materials Project [1] and the Inorganic Crystal Structure Database (ICSD) [2,3] enable the screening of a wide range of two-dimensional (2D) materials potentially characterized by excellent electrochemical performance in a range of battery chemistries [4,5,6]. Among the different technologies under development, lithium-sulfur (Li-S) batteries are particularly promising due to their high theoretical energy density (2600 Wh kg^{-1}) and the abundance, low cost, and safety of sulfur [7,8,9]. However, drawbacks such as the poor interfacial stability of Li anodes and the migration of intermediate lithium polysulfide (LiPS) species Li_2S_x (x = 1, 2, 4, 6, and 8) hamper the commercialization of this technology [10.11]. To overcome Li-S battery flaws, at the cathode side, considerable efforts have been devoted to improving the electrical conductivity of sulfur cathodes, promoting the physical sequestration and chemical adsorption of LiPs, and accelerating the Li-S redox reaction kinetics [12-16]. 2D transition metal compounds, including sulfides, carbides, phosphides, and nitrides, offer abundant polar sites for strong chemical interaction with LiPSs, excellent electrical conductivities, and outstanding Li-S electrocatalytic properties [16-20]. Therefore, when used as an additive in the S cathode, they result in Li-S batteries with significantly improved electrochemical performances.

MXenes, offering high specific surface areas, excellent metallic conductivity, and rich functional terminations, are a paradigmatic example of the potential of 2D transition metal compounds in the field of electrochemistry [18,21-28]. 2D transition metal phosphides (TMPs) are an emerging class of 2D material that has been largely overlooked despite their potential in the field of catalysts, thermal insulation,

optoelectronics, and magnetism [29,30].

We hypothesize that, within the 2D TMP family, some specific compositions may offer excellent performance as cathode additives in Li-S batteries. To probe this and address the current lack of research on 2D TMPs, we have screened a large range of TMP compositions using the ICSD database. We have found two 2D TMPs, Zr_2PS_2 and Zr2PTe$_2$, with structural similarities to MXenes. First-principles calculations have shown that Zr_2PS_2 and Zr_2PTe_2 are characterized by excellent metallic conductivities, notable LiPS adsorption energy to suppress their migration, high Li ion diffusivity, and reduced Li_2S decomposition and LiPS nucleation energy barriers. Simultaneously, we further analyze the potential suitability of Zr_2PS_2 and Zr_2PTe_2 as Li-S catalysts using electron localization function (ELF), charge density difference (CDD), and localized orbital locator (LOL) methods.

We have screened a wide range of 2D TMPs and MAP (M = transition metals; A = main group IIIA to VA element) phases from the ICSD database using first-principles modeling (Figure 1a). From this initial screening, we identified two promising 2D TMPs — Zr_2PS_2 and Zr_2PTe_2— as potential additives for Li-S batteries' sulfur cathodes [31]. Zr_2PS_2 initially forms Zr_2P by removing Sb atoms from the precursor compound Zr_2SbP [32]. The specific screening process and criteria were as follows: First, we focused on 2D TMPs because the layered structure enables the material to possess advantages such as a large specific surface area and unique electronic properties. In addition, TMPs exhibit excellent electrical conductivity and electrochemical catalysis activity [33, 34]. Because MXenes-based electrode materials have demonstrated

excellent performance in Li-S batteries, the scope of selection was further narrowed down to 2D TMPs with similar structures and identical chemical formulas to MXenes. Additionally, since the primary method of obtaining MXenes materials involves chemically etching MAX to remove the interlayer, we also aimed at MAX phases [35]. After determining the target composition and elements, we searched the ICSD database with rich resources and comprehensive structural information. We entered relevant keywords into the database, such as material type, performance parameters, and chemical composition, and then examined the detailed information of the filtered materials to determine if they met the criteria.

Zr_2PS_2 and Zr_2PTe_2 crystallize in the hexagonal space group *P*63/*mmc* (No. 194) and the trigonal space group *R*3-*m* (No. 166), respectively. These two structures exhibit a high degree of similarity, with a P layer sandwiched between two Zr layers and the outermost layers being S and Te layers. The Z values of these two structures are 2 and 3, respectively. In Zr_2PS_2, the combined thickness of the P layer and the two Zr layers is approximately 2.91 Å. Notably, the outermost S atoms prefer the sites directly above the Zr atoms of the lower layer. The nearest distance between the Zr and sulfur layers is 1.45 Å. Each P atom coordinates with six Zr atoms, while each Zr atom coordinates with three inner P atoms and three S atoms. The lengths of the Zr-P and Zr-S bonds are 2.64 and 2.52 Å, respectively (**Figure. 1b**). In Zr_2PTe_2, both phosphide and telluride anions, are arranged in layers. These layers stack along the *c*-axis in a specific sequence: two layers of telluride ions followed by one layer of phosphide ions. The octahedral vacancies between the phosphide and telluride layers are occupied by zirconium cations.

Notably, the voids between neighboring telluride layers remain completely empty, resulting in a sandwich-like arrangement [Te-Zr-P-Zr-Te] (**Figure. 1c**). Since the structure of Zr_2PTe_2 is already known through experiments, here we only evaluate the dynamic stability of the new artificial structure Zr_2PS_2 through calculating the phonon spectrum (as presented in **Figure 1d**). Importantly, no virtual frequencies were observed, confirming its dynamic stability.

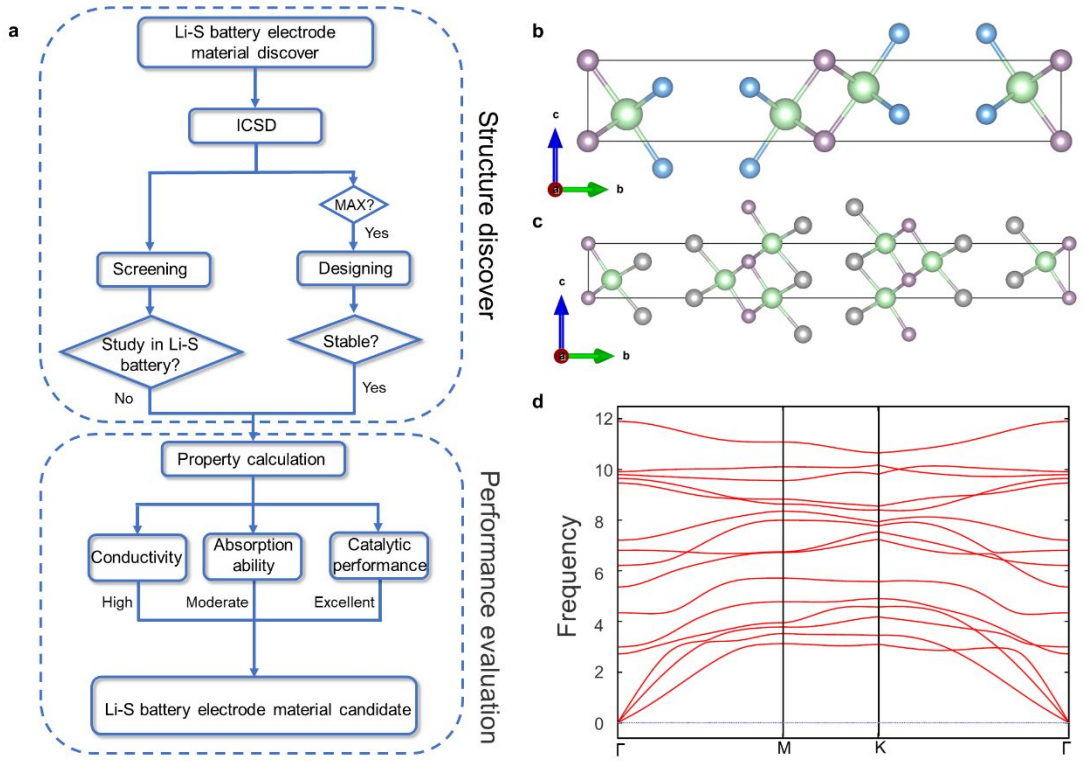

Figure. 1: (a) Workflow of first-principles screening and designing. (b) Structural features of Zr_2PS_2 and Zr_2PTe_2. Zr (light green spheres), P (light purple spheres), S (blue spheres), and Te (gray spheres). (c) Phonon dispersion spectra of Zr_2PS_2.

One key characteristic of a suitable electrocatalyst for accelerating electrochemical reactions in a Li-S battery is high electrical conductivity. To investigate the charge transport abilities of Zr_2PS_2 and Zr_2PTe_2, we calculated their electronic band structures, focusing on the density of states (DOS), using DFT (**Figures 2a,b**). Both materials,

Zr_2PS_2 and Zr_2PTe_2, exhibit the Fermi level situated within a band of states, indicative of a metallic character. Specifically for Zr_2PS_2, the partial and total DOS reveal that Zr-4*d* and S-3*p* orbitals significantly contribute to the band of states at the Fermi level. Similarly for Zr_2PTe_2, the DOS analysis shows that Zr-4*d* and Te-5*p* orbitals play a crucial role in shaping the electronic structure near the Fermi level. To further elucidate the bonding nature of Zr_2PS_2 and Zr_2PTe_2, we calculated their ELF (**Figures 2c,d**). Interestingly, the ELF values for both compounds are close to 1 for Zr/P/S atoms, indicating highly localized bonding. However, no significant electron localization was observed on the Zr-P and Zr-S bonds or the Zr-Te bonds, consistent with their overall metallic behavior.

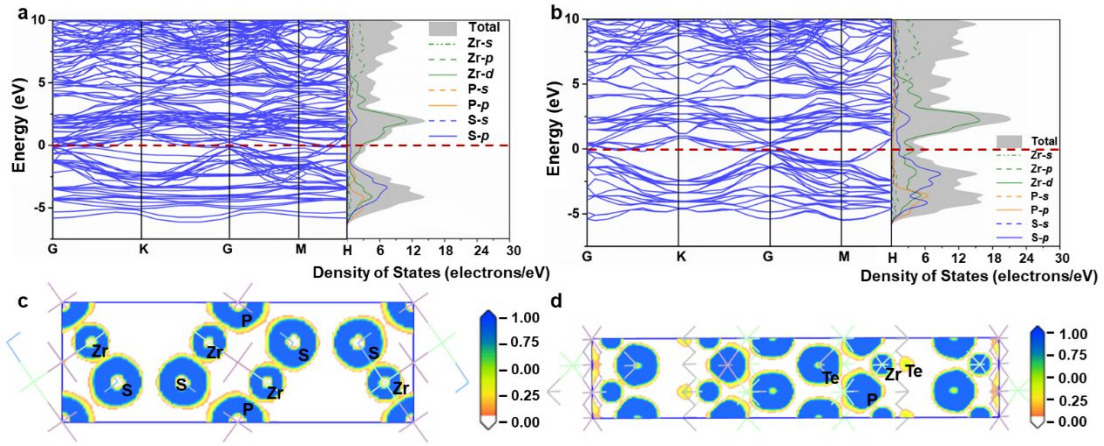

Figure 2. (a, b) Band structure and partial and total DOS of Zr_2PS_2 and Zr_2PTe_2, respectively, showing no band gap at the Fermi level. (c, d) ELF of Zr_2PS_2 and Zr_2PTe_2, respectively.

The performance of Li-S batteries is also strongly dependent on the ability of the electrode material to adsorb Li_2S_x species. A significant adsorption energy is a necessary condition to trap LiPS and prevent their migration to the anode side. To determine the most stable structures, we strategically placed the Li_2S_x species at

different positions on the surfaces of Zr_2PS_2 (001) and Zr_2PTe_2 (001) (Figure S1). For instance, when considering Li_2S, the most favorable adsorption sites comprise S-Top, S-Down, and Li-Side (Figure S1). The corresponding adsorption energies at these three sites on Zr_2PS_2 are −3.05 eV, −3.04 eV, and −1.14 eV, respectively. The most stable adsorption sites for Li_2S_x species and S_8 on the Zr_2PS_2 (001) and Zr_2PTe_2 (001) surfaces were also calculated and shown in **Figures 3a** and S2. The ring structure of the S_8 molecule remains intact and is parallel to the surfaces of Zr_2PS_2 (001) and Zr_2PTe_2 (001), and the adsorption energies are −0.31 eV and −0.47 eV, respectively. For insoluble Li_2S and Li_2S_2, the Li atoms tend to combine with the terminations of the Zr_2PS_2 (001) and Zr_2PTe_2 (001) surfaces. The adsorption energies of Li_2S and Li_2S_2 on the Zr_2PS_2 (001) surface are −3.05 eV, and −0.84 eV, respectively. The adsorption energies of Li_2S and Li_2S_2 on the Zr_2PTe_2 (001) surface are −2.98 eV and −0.68 eV, respectively. As for the soluble Li_2S_4, Li_2S_6, and Li_2S_8, similar to the insoluble Li_2S and Li_2S_2, Li atoms tend to combine with S or Te atoms of the Zr_2PS_2 (001) and Zr_2PTe_2 (001) surface. On the surface of Zr_2PS_2 (001), the adsorption energies of Li_2S_4, Li_2S_6, and Li_2S_8 are −0.51 eV, −0.48 eV, and −1.07 eV, respectively. On the other hand, when adsorbed on the Zr_2PTe_2 (001) surface, their adsorption energies are −0.41 eV, −0.50 eV, and −1.08 eV, respectively. Overall, Zr_2PS_2 and Zr_2PTe_2 are characterized by notable adsorption energies for Li_2S_x, ranging from −0.31 eV to −3.05 eV and −0.41 eV to −2.98 eV, respectively. These research results indicate that Zr_2PS_2 and Zr_2PTe_2 can effectively anchor Li_2S_x, potentially inhibiting their dissolution and migration, as well as activating their electrocatalytic conversion.

The anchoring mechanism of Zr_2PS_2 and Zr_2PTe_2 was further analyzed through CDD. **Figure 3b** and S3,4 shows the CDD between Li_2S_x species and Zr_2PS_2 and Zr_2PTe_2. The cyan regions indicate the accumulation of charge, and the orange regions indicate the depletion of charge. Statistical analysis on EDD was conducted to quantify the accumulation and depletion of charges (**Figures 3c** and S5). When the S_8 molecule is adsorbed on the Zr_2PS_2 (001) surface, charge transfer occurs inside the S_8 molecule and inside Zr_2PS_2, respectively, but almost no charge exchange takes place between the S_8 and Zr_2PS_2 (**Figures 3c**, and S3). This indicates that the main interaction between S_8 and the Zr_2PS_2 (001) surface is through van der Waals forces, which is consistent with our results on the adsorption energy. With the lithiation of Li_2S_8 to Li_2S, the accumulation and depletion of charges between the Zr_2PS_2 (001) surface and Li_2S_x become increasingly intense (Figure 3c). As shown in Figure 3c, charge transfer is not the only factor that determines the adsorption energy. Although there is not much difference in charge transfer between Li_2S and the Zr_2PS_2 (001) surface compared with other polysulfides, the short adsorption distance and bond length between Li_2S and the Zr_2PS_2 (001) surface (Figure S6 and Table S1) make it more difficult for Li_2S to desorb from the Zr_2PS_2 surface [36, 37]. In addition, the internal charge loss of Li_2S_x (orange regions) leads to softening of the Li–S bond, which facilitates to the conversion of Li_2S_x. Similar results were obtained for Zr_2PTe_2.

The diffusibility of Li ions within the electrode material significantly impacts the charge/discharge rate in Li-S batteries. Consequently, we conducted a thorough study on the diffusibility of Li ions on the Zr_2PS_2 (001) and Zr_2PTe_2 (001) surfaces. Our

approach involved considering diffusion paths from the most stable site to the second stable site and back to the most stable site. Specifically, we explored three different Li adsorption sites on these surfaces: the apex positions of the Zr atom, P atom, and S atom/Te atom (as illustrated in Figure S7). After geometric optimization, we identified the following stable sites for Li ion adsorption:

- In the case of Zr_2PS_2, the most stable site corresponds to the vertex position of P atom, while the second stable site aligns with the vertex position of the Zr atom (as depicted in Figure S8a).
- However, in the case of Zr_2PTe_2, the most stable site is located at the vertex position of Zr, while the second stable site corresponds to the vertex position of the P atom (as shown in Figure S8b).

Furthermore, we analyzed the diffusion paths and potential barriers for Li ions on Zr_2PS_2 and Zr_2PTe_2 as shown in Figures 3d,e,f. Interestingly, we observed relatively little diffusion energy barriers for Li ions on both materials, which should favor reaching a high charge/discharge rate.

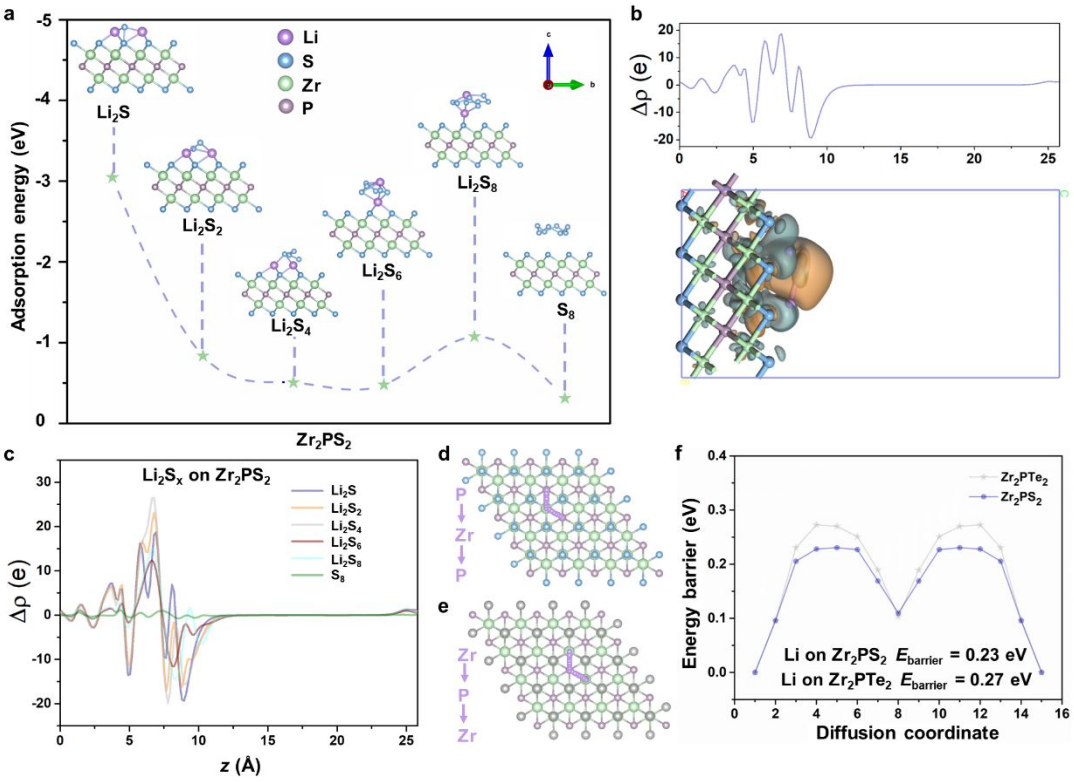

Figure 3. (a) Adsorption energies for a series of sulfur-related species on the Zr_2PS_2 (001) surface. (b) CDD after binding of a Li_2S species on a Zr_2PS_2; cyan (orange) denotes charge gain (loss). The isosurface level is set to 0.05 e/Å^3. (c) Plane CDD along the *z*-axis between a Li_2S_x molecule and Zr_2PS_2. (d, e) Diffusion pathways of Li ion on Zr_2PS_2 and Zr_2PTe_2, respectively. (f) Diffusion barriers of Li ion on Zr_2PS_2 and Zr_2PTe_2, respectively.

A significant drawback of Li-S batteries is the low electrical conductivity, reduced Li ion diffusivity, and the high decomposition potential of the final discharge product, Li_2S. These properties contribute to a high overpotential and low-rate performance. To gain insights into the Li_2S decomposition mechanism on Zr_2PS_2 and Zr_2PTe_2, we conducted additional calculations.

The decomposition process involves breaking down the original Li_2S molecule into LiS and a Li^+ ion, i.e. $Li_2S \rightarrow LiS + Li^+ + e^-$. Notably, Li_2S exhibits small decomposition barriers of 0.79 eV and 1.2 eV, on Zr_2PS_2 and Zr_2PTe_2 respectively (as shown in Figure

4a). This suggests a strong catalytic ability of both Zr_2PS_2 and Zr_2PTe_2 in facilitating Li_2S decomposition. To clarify why the decomposition barrier of Li_2S on Zr_2PS_2 is significantly lower than on Zr_2PTe_2, we analyzed the electronic wave function of Li_2S on both materials using the Multiwfn package [38]. Specifically, Figures 4 b,c depict the LOL of Li_2S on Zr_2PS_2 and Zr_2PTe_2, respectively, in the plan view. Additionally, we employed ELF calculations to examine the bonding characteristics between Li and S/Te in these structures. As shown in Figures 4 d,f, the two Li atoms in Li_2S form an ionic bond with the S atom in Zr_2PS_2, whereas the Li atom in Li_2S and the Te atom in Zr_2PTe_2 form a covalent bond. Since covalent bonds are stronger than ionic bonds, higher energy is required to break them. This difference in bonding nature accounts for the significantly lower decomposition barrier of Li_2S on Zr_2PS_2 compared to Zr_2PTe_2.

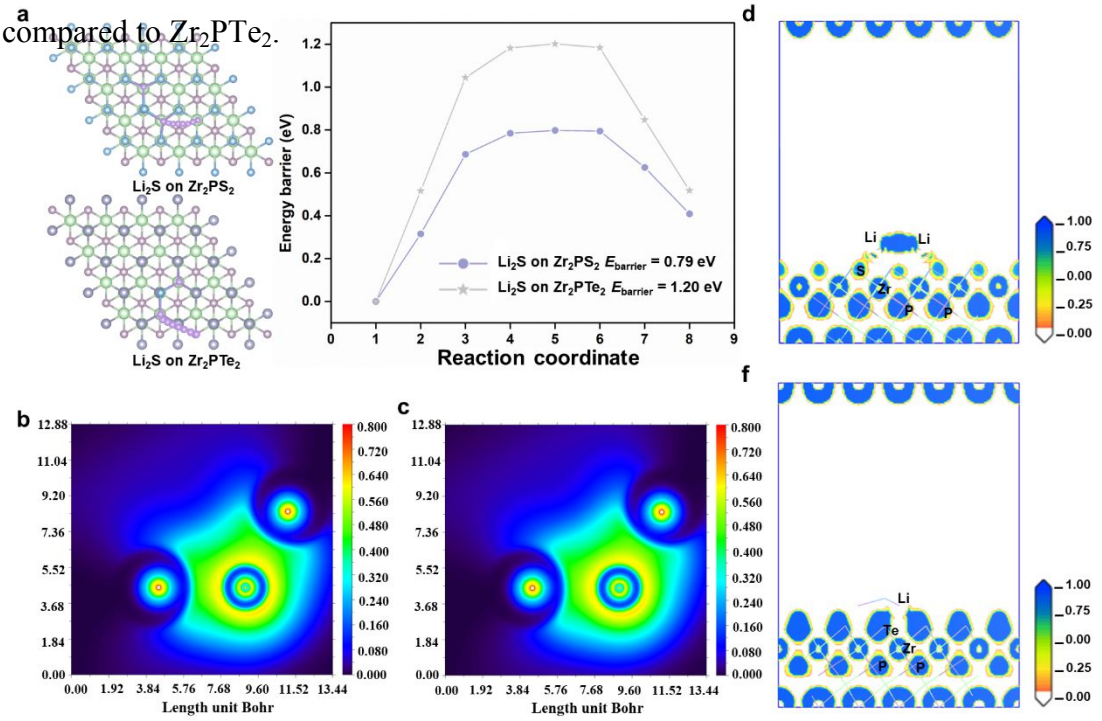

Figure 4. (a) Dissociation barrier and pathway of Li_2S cluster on Zr_2PS_2 and Zr_2PTe_2, respectively. (b, c) LOL of Li_2S on Zr_2PS_2 and Zr_2PTe_2, respectively. (e, f) ELF of Li_2S species on Zr_2PS_2 and Zr_2PTe_2, respectively.

The Gibbs free energy changes of the reaction steps from S_8 to Li_2S on the Zr_2PS_2 and Zr_2PTe_2 substrates were investigated through first-principles calculations. The relative energy evolution curve of the reaction process is shown in Figure S9. Except for the first step of spontaneous exothermic conversion from S_8 to Li_2S_8, the subsequent gradual formation of lithium polysulfides is an endothermic process. The largest free energy difference among all reaction steps is the rate-limiting step in the sulfur redox reaction process. The Gibbs free energy calculation results indicate that the sulfur reduction process on the surfaces of Zr_2PS_2 and Zr_2PTe_2 has thermodynamic advantages. We introduce Crystal Orbital Hamilton Population (COHP) to analyze the reasons for the excellent catalytic polysulfide conversion ability of Zr_2PS_2. The integrated value of COHP (-ICOHP) is calculated by integrating the corresponding energy below the Fermi level (E_f). A larger value of -ICOHP indicates a stronger interaction between atoms. As shown in Figure S10, the -ICOHP values of Li/S-S bonds in Zr_2PS_2-Li_2S and Zr_2PS_2-Li_2S_2 are 1.54 (Li_2S), 1.36 (Li_2S_2), respectively. As electrode materials for Li-S batteries, it is necessary to possess high electrical conductivity, moderate adsorption capacity, and strong catalytic activity simultaneously. These properties working together can ensure that Li-S batteries have faster reaction rates, higher energy efficiency, and stable cycling performance. Compared to metal carbides, nitrides, and oxides, metal phosphides have a relatively moderate adsorption capacity for LiPSs, but they demonstrate certain advantages in terms of conductivity and catalytic performance (Tables S2 and S3).

In this work, we have conducted an extensive screening of materials from the ICSD

database and identified Zr_2PS_2 and Zr_2PTe_2 as suitable catalytic additives in the S cathode of Li-S batteries. These new artificial crystal structures were designed based on the existing Zr_2SbP structure. To assess the dynamic stability of Zr_2PS_2, we calculated its phonon spectrum. Furthermore, we performed first-principles calculations to investigate the performance of Zr_2PS_2 and Zr_2PTe_2 as electrode materials for Li-S batteries. Theoretical evaluations revealed that Zr_2PS_2 and Zr_2PTe_2 can improve the conductivity of the S cathode and enhance the electrochemistry performance of Li-S batteries. $Zr2PS_2$ and Zr_2PTe_2 can block the migration of polysulfides, and enhance the Coulombic efficiency and cycling stability of Li-S batteries. Additionally, Zr_2PS_2 and Zr_2PTe_2 can regulate the dynamic behavior of Li ions due to their unique ion-sieving effect, effectively stabilizing the deposition/stripping of lithium. Zr_2PS_2 and Zr_2PTe_2 exhibit significantly improved electrocatalytic functions on the nucleation and decomposition kinetics of Li_2S, which can endow Li-S batteries with excellent rate performance and cycling stability. These computational results strongly suggest that Zr_2PS_2 and Zr_2PTe_2 are potentially outstanding electrode materials not only for Li-S batteries, but also for other fields such as optoelectronics and catalysis. The above results indicate that this material screening method can accelerate the discovery of new structures, and this method can also be applied to other functional material fields. In addition, machine learning methods can also be used in the material screening process to assist high-throughput screening of properties and dynamic analysis.

Supporting Information

The supporting information is available free of charge via the Internet. Experimental suggestions, first-principles calculations methods, optimized structures and the corresponding adsorption energies, calculated adsorption energy, calculated adsorption energy of Zr_2PTe_2, charge density difference analysis, quantify the accumulation and depletion of charges, statistically the bond lengths, the adsorption sites of Li ions on Zr_2PS_2 and Zr_2PTe_2, the most stable and second stable adsorption sites of Li ions on Zr_2PS_2 and Zr_2PTe_2, calculated Gibbs free energy, COHP analysis, the shortest distances (d) between lithium polysulfides and S_8 with the Surfaces of Zr_2PS_2 and Zr_2PTe_2, The adsorption energy band gap, Li_2S decomposition barrier and Li ion diffusion barrier of Ti_2NS_2, Zr_2CO_2, C@WS_2/S, Zr_2NO_2, 2H-MoS_2, D-TiO_2, Zr_2PS_2 and Zr_2PTe_2 adsorbing lithium polysulfides and S_8.

Declaration of competing interest

The authors declare that they have no known competing financial interests or personal relationships that could have appeared to influence the work reported in this paper.

Corresponding Author

Email: dwyang@henu.edu.cn

Email: acabot@irec.cat

Acknowledgements

The authors acknowledge support from the 2BoSS project of the ERA-MIN3 program with the Spanish grant number PCI2022-132985/AEI/10.13039/501100011033 and the

SyDECat project from the Spanish MCIN/AEI/FEDER (PID2022-136883OB-C22). The authors thank the support from the project NANOGEN (PID2020-116093RB-C43), funded by MCIN/ AEI/10.13039/501100011033/ and by "ERDF A way of making Europe", by the "European Union". ICN2 and IREC acknowledges funding from Generalitat de Catalunya 2021SGR00457 and 2021SGR01581 and European Union NextGenerationEU/PRTR. This study is part of the Advanced Materials programme and was supported by MCIN with funding from European Union NextGenerationEU (PRTR-C17.I1) and by Generalitat de Catalunya. ICN2 is supported by the Severo Ochoa program from Spanish MCIN / AEI (Grant No.: CEX2021-001214-S) and is funded by the CERCA Programme / Generalitat de Catalunya. D. Yang thanks the China Scholarship Council for the scholarship support and the funding from the National Natural Science Foundation of China (NSFC) (Grants No. 22305064).

References

[1] Jain, A.; Ong, S. P.; Hautier, G.; Chen, W.; Richards, W. D.; Dacek, S.; Cholia, S.; Gunte, D.; Skinner, D.; Ceder, G.; Persson, K. A. Commentary: The materials project: A materials genome approach to accelerating materials innovation. *APL Mater.* **2013,** *1,* 011002.

[2] Hellenbrandt, M. The Inorganic Crystal Structure Database (ICSD)—present and future. *Crystallogr. Rev.* **2004,** *10,* 17–22.

[3] Belsky, A.; Hellenbrandt, M.; Karen, V. L.; Luksch, P. New developments in the Inorganic Crystal Structure Database (ICSD): Accessibility in support of materials research and design. *Acta Crystallogr. B Struct. Sci.* **2002,** *58,* 364–369.

[4] Merchant, A.; Batzner, S.; Schoenholz, S. S.; Aykol, M.; Cheon, G.; Cubuk, E. D. Scaling deep learning for materials discovery. *Nature* **2023,** *624,* 80–85.

[5] Zhou, G. M.; Zhao, S. Y.; Wang, T. S.; Yang, S.-Z.; Johannessen, B.; Chen, H.; Liu,

C. W.; Ye, Y. S.; Wu, Y. C.; Peng, Y. C.; Liu, C.; Jiang, S. P.; Zhang, Q. F.; Cui, Y. Theoretical calculation guided design of single-atom catalysts toward fast kinetic and long-life Li–S batteries. *Nano Lett.* **2020,** *20,* 1252–1261.

[6] Olsson, E.; Yu, J.; Zhang, H.; Cheng, H. M.; Cai, Q. Atomic-scale design of anode materials for alkali metal (Li/Na/K)-ion batteries: Progress and perspectives. *Adv. Energy Mater.* **2022,** *12,* 2200662.

[7] Service, R. F. Lithium-sulfur batteries poised for leap. *Science* **2018,** *359,* 1080–1081.

[8] Manthiram, A.; Chung, S. H.; Zu, C. Lithium–sulfur batteries: Progress and prospects. *Adv. Mater.* **2015,** *27,* 1980–2006.

[9] Zhang, Y.; Zhang, X.; Silva, S. R. P.; Ding, B.; Zhang, P.; Shao, G. S. Lithium–sulfur batteries meet electrospinning: recent advances and the key parameters for high gravimetric and volume energy density. *Adv. Sci.* **2022,** *9,* 2103879.

[10] Hu, A.; Zhou, M.; Lei, T.; Hu, Y.; Du, X.; Gong, C.; Shu, C.; Long, J.; Zhu, J.; Chen, W.; Wang, X.; Xiong, J. Optimizing redox reactions in aprotic lithium–sulfur batteries. *Adv. Energy Mater.* **2020,** *10,* 2002180.

[11] Zhao, M.; Li, B.-Q.; Peng, H.-J.; Yuan, H.; Wei, J.-Y.; Huang, J.-Q. Lithium–sulfur batteries under lean electrolyte conditions: challenges and opportunities. *Angew. Chem. Int. Ed.* **2020,** *59,* 12636.

[12] Yang, D. W.; Liang, Z. F.; Tang, P. Y.; Zhang, C. Q.; Tang, M. X.; Li, Q. Z.; Biendicho, J. J.; Li, J.; Heggen, M.; Dunin-Borkowski, R. E.; Xu, M.; Llorca, J.; Arbiol, J.; Morante, J. R.; Chou, S.-L.; Cabot, A. A high conductivity 1D π–d conjugated metal–organic framework with efficient polysulfide trapping-diffusion-catalysis in lithium–sulfur batteries. *Adv. Mater.* **2022,** *34,* 2108835.

[13] Zhang, Y.; Zhang, P.; Zhang, S.; Wang, Z.; Li, N.; Silva, S. R. P.; Shao, G. A flexible metallic TiC nanofiber/vertical graphene 1D/2D heterostructured as active electrocatalyst for advanced Li-S batteries. *InfoMat.* **2021,** *3,* 790–803.

[14] Liu, Z. F.; Chen, M.; Zhou, D.; Xiao, Z. B. Scavenging of "dead sulfur" and "dead Lithium" revealed by integrated–heterogeneous catalysis for advanced lithium–sulfur

batteries. *Adv. Funct. Mater.* **2023,** *33,* 2306321.

[15] Zhou, W. Y.; Lin, J.-X.; Tang, Y. X.; Sheng, T.; Deng, Y. H.; Tan, Y. L.; Mo, Y. X. Catalyst for polysulfide conversion by Mo_2C/MoO_3 hybrids modified separator in lithium-sulfur batteries. *Mater. Today Phys.* **2023,** *37,* 101193.

[16] Shen, Z.; Jin, X.; Tian, J.; Li, M.; Yuan, Y.; Zhang, S.; Fang, S.; Fan, X.; Xu, W.; Lu, H.; Lu, J.; Zhang, H. Cation-doped ZnS catalysts for polysulfide conversion in lithium–sulfur batteries. *Nat. Catal.* **2022,** *5,* 555–563.

[17] Cheng, Z.; Xiao, Z.; Pan, H.; Wang, S.; Wang, R. Elastic sandwich-type rGO-VS_2/S composites with high tap density: structural and chemical cooperativity enabling lithium-sulfur batteries with high energy density. *Adv. Energy Mater.* **2018,** *8,* 1702337.

[18] Gogotsi, Y.; Anasori, B. The rise of MXenes. *ACS nano* **2019,** *13,* 8491–8494.

[19] Guo, Z.; Zhou, J.; Sun, Z. New two-dimensional transition metal borides for Li ion batteries and electrocatalysis. *J. Mater. Chem. A* **2017,** *5,* 23530–23535.

[20] Miao, N. X.; Gong, Y. T.; Zhang, H. Y.; Shen, Q.; Yang, R.; Zhou, J. P.; Hosono, H.; Wang, J. J. Discovery of two-dimensional hexagonal MBene HfBO and exploration on its potential for lithium-ion storage. *Angew. Chem. Int. Ed.* **2023,** *62,* e202308436.

[21] Wei, C.; Xi, B.; Wang, P.; Liang, Y.; Wang, Z.; Tian, K.; Feng, J.; Xiong, S. In situ anchoring ultrafine ZnS nanodots on 2D MXene nanosheets for accelerating polysulfide redox and regulating Li plating. *Adv. Mater.* **2023,** *35,* 2303780.

[22] Lieu, W. Y. Lin, C. Li, X. L. Jiang, S. Li, Y. Yang, H. She, Z. W. Structural design of electrocatalyst-decorated MXenes on sulfur spheres for lithium-sulfur batteries. *Nano Lett.* **2023,** *23,* 5762–5769.

[23] Chen, L.; Sun, Y.; Wei, X.; Song, L.; Tao, G.; Cao, X.; Wang, D.; Zhou, G.; Song, Y. Dual-functional V_2C MXene assembly in facilitating sulfur evolution kinetics and Li-Ion sieving toward practical lithium-sulfur batteries. *Adv. Mater.* **2023,** *35,* 2300771.

[24] Xiong, D.; Shi, Y.; Yang, H. Rational design of MXene-based films for energy storage: Progress, prospects, *Mater. Today* **2021,** *46,* 183–211.

[25] Liao, L.; Wang, S.; Duan, H.; Deng, Y. MXene-based materials: Synthesis, structure and their application for advanced lithium-sulfur batteries, *J. Energy Storage*

2024, *75,* 109555.

[26] Gonçalves, J. M.; Santos, É.A.; Martins, P. R.; Silva, C. G.; Zanin, H. Emerging medium- and high-entropy materials as catalysts for lithium-sulfur batteries. *Energy Storage Mater.* **2023,** 75, 102999.

[27] Song, C.; Zhang, W.; Jin, Q.; Zhao, Y.; Zhang, Y.; Wang, X.; Bakenov, Z. Oxidized Nb_2C MXene as catalysts for lithium-sulfur batteries: Mitigating the shuttle phenomenon by facilitating catalytic conversion of lithium polysulfides. *J. Mater. Sci. Technol.* **2022,** *119,* 45–52.

[28] Liu, X.; Shao, X.; Li, F.; Zhao, M. Anchoring effects of S-terminated Ti_2C MXene for lithium-sulfur batteries: A first-principles study. *Appl. Surf. Sci.* **2018,** *455,* 522–526.

[29] Shao, Y.; Shi, X.; Pan, H. Electronic, magnetic, and catalytic properties of thermodynamically stable two-dimensional transition-metal phosphides. *Chem. Mater.* **2017,** 29, 8892–8900.

[30] Ying, Y.; Fan, K.; Luo, X.; Huang, H. Predicting two-dimensional pentagonal transition metal monophosphides for efficient electrocatalytic nitrogen reduction. *J. Mater. Chem. A* 2019, *7,* 11444–11451.

[31] Tschulik, K.; Ruck, M.; Binnewies, M.; Milke, E.; Hoffmann, S.; Schnelle, W.; Fokwa, B.P.T.; Gillessen, M.; Schmidt, P. Chemistry and physical properties of the phosphide telluride Zr_2PTe_2. *Eur. J. Inorg. Chem.* **2009,** *21,* 3102-3110.

[32] Boller, H. Gemischte pnictide mit geordnetem TiP-Typ (Ti_2SC-Typ). *Monatsh. Chem.* **1973,** *104,* 166-171.

[33] Shao, Y.; Shi, X.; Pan, H. Electronic, magnetic, and catalytic properties of thermodynamically stable two-dimensional transition-metal phosphides. *Chem. Mater.* **2017,** *29,* 8892–8900.

[34] Ying, Y.; Fan, K.; Luo, X.; Huang, H. Predicting two-dimensional pentagonal transition metal monophosphides for efficient electrocatalytic nitrogen reduction. *J. Mater. Chem. A* **2019,** *7,* 11444–11451.

[35] Naguib, M.; Barsoum, M.W.; Gogotsi, Y. Ten years of progress in the synthesis

and development of MXenes. *Adv Mater,* **2021,** *33,* e2103393.

[36] Zhao, W.; Xu, L-C.; Guo, Y.; Yang, Z.; Liu, R.; Li, X. TiS_2-graphene heterostructures enabling polysulfide anchoring and fast electrocatalyst for lithium-sulfur batteries: A first-principles calculation. *Chinese Phys. B* **2022,** *31,* 047101.

[37] Zhao, W.; Xu, L-C.; Li, R.; Guo, Y.; Yang, Z.; Liu, R.; Li X. Enhance the anchoring and catalytic performance of lithium-sulfur batteries for lithium polysulfide by predicted TiS_2 monolayer. *Mater. Today Commun.* **2022,** *30,* 103196.

[38] Lu, T.; Chen, F. Multiwfn: A multifunctional wavefunction analyzer. *J. Comput. Chem.*, **2012,** *33,* 580–592.

Abstract Graphics